

CAAP Quarterly Report

Date of Report: January 10th 2020

Prepared for: *U.S. DOT Pipeline and Hazardous Materials Safety Administration*

Contract Number: 693JK31850008CAAP

Project Title: Fluorescent Chemical Sensor Array for Detecting and Locating Pipeline Internal Corrosive Environment

Prepared by: Dr. Ying Huang, Dr. Wenfang Sun, and Dr. Hao Wang

Contact Information: Dr. Ying Huang, Email: ying.huang@ndsu.edu, Phone: 701.231.7651

For quarterly period ending: January 10th 2020

Business and Activity Section

(a) Contract Activity

Discussion about contract modifications or proposed modifications

None.

Discussion about materials purchased

None.

(b) Status Update of Past Quarter Activities

Task 2.1, 2.2, 2.3, Task 3

(c) Cost share activity

None (Reported last quarter).

(d) Task 2: Development of Fluorescent/Colorimetric Chemical Sensor Array for Internal Corrosive Water Detection

Four subtasks were worked on during this quarter including Task 2.1 (Development of Fluorescent/Colorimetric Chemical Sensor Array), Task 2.2 (Calibration of the Fluorescent/colorimetric Chemical Sensor Array), Task 2.3 (Optimization of The Colorimetric/Fluorescent Chemical Sensor Array and Its Corresponding Network), and Task 3 (Integration of Corrosive Water into Internal Corrosion Prediction Models). The detail findings are described as below:

1. Background and Objectives in the 5th Quarter

1.1 Background

This project is designed to develop passive colorimetric/fluorescent chemical sensor array for locating and detecting corrosive water inside pipes. Inside the pipelines, the transported crude oil may include a hot

mixture of free water, carbon dioxide (CO₂), hydrogen sulfide (H₂S) and microorganisms. The different chemical components inside oil/water environment such as HCO₃⁻ / CO₃²⁻, Fe³⁺, S²⁻, H⁺ or pH may result in different internal corrosion mechanisms, such as sweet corrosion or sour corrosion. The passive colorimetric sensor array to be developed in this project is intended to detect the concentration changes of the five above mentioned important chemical species in the internal oil/water environment of the pipeline and use these detected environmental data to predict the internal corrosion progressing of pipelines.

1.2 Objectives in the 5^h Quarter

In this quarter, we would write the sensor into several different porous polymeric matrix to find the material which could work to host the sensor (the PMMA, CA, and PMMA/CA), conduct CFD analysis of the pipeline with sensors attached in water/oil environment, conduct lab experiments to test the survivability of the sensor under regular oil/gas environment, under pigging service (cleaning), and validate the FEM model to optimize the sensor's thickness based on the pigging service, and based on the test results. In addition, corrosion models for internal corrosion analysis is reviewed and the model to be used for corrosion modeling is selected followed by test plans on quantifying several uncertain effects which will be detected from the sensors.

2. Results and Discussions

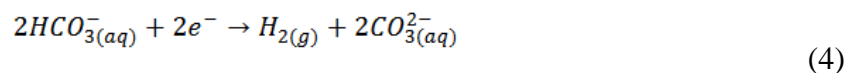
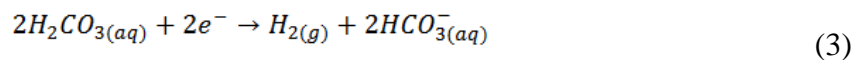
In last quarter, PMMA with embedded sensor successfully detected the Fe²⁺ ion. Based on the corrosion principle of the sweet corrosion, the presence of Fe²⁺ is because of the chemical reaction between the CO₂, water, and Fe, inducing a chemical product of iron carbonate (FeCO₃) following the chemical reaction below [1]:



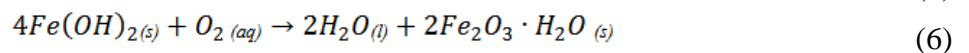
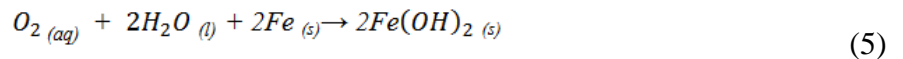
Accordingly, it can be seen that the detection of the Fe²⁺ can be used to represent the detection of CO₃²⁻. In addition, in an acidic solution, hydrogen ions (H⁺) diffuse to the steel surface to receive the electrons released by the iron via the following reduction reaction:



This reduction results in hydrogen gas evolution. Other reduction reactions involving carbonates also existed, known as the 'direct' reduction of carbonic acid and bicarbonate ion, respectively [2], [3] as:



From the above chemical reaction, it can be found out that the existing of the CO₃²⁻ ion is a result of the formulation of HCO₃⁻. Thus, the detection of the H⁺ and CO₃²⁻ ion and their concentration ranges can obtain a good understanding of the presentence of the HCO₃⁻ ion. Thus, in the future quarters, the target detection of the ions remains as Fe³⁺, S²⁻, and H⁺/pH. In this quarter, we have successfully detected Fe³⁺ using PMMA/CA film with embedded sensor, which is an indication of presence of oxygen in the gas/oil mixture as shown in the following chemical reactions [1]:



Thus, based on the potential internal corrosion mechanism as shown in Fig. 1, the influence of CO₃²⁻/Fe²⁺ on the chemical reaction of sweet corrosion and the effect of oxygen can be investigated using the developed sensors. However, in this quarter, the detection S²⁻ was still not successful and the detection of H⁺/pH is

still uncertain by the end of this quarter. Thus, in next quarter, we will focus on testing the sensing ability of the PMMA/CA film for H^+ /pH and developing another sensor film to detect S^{2-} ion.

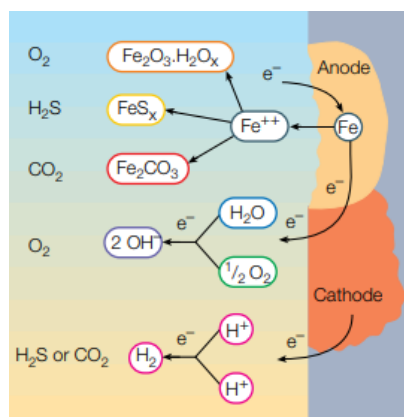


Fig. 1. Internal corrosion mechanism

2.1 Development of Fluorescent/Colorimetric Chemical Sensor Array (Task 2.1) and Calibration of the Fluorescent/colorimetric Chemical Sensor Array (Task 2.2)

In this quarter, we did the planned study on selecting and testing some other porous polymeric materials (including PMMA (poly(methyl methacrylate) Isotactic), CA (cellulose acetate), and PMMA/CA polymer films) for the sensor matrix for Fe^{3+} and S^{2-} , and testing the sensitivity and resolution of sensor if sensor is successfully developed. The results showed that in addition to Fe^{2+}/CO_3^{2-} which was developed successfully in last quarter, the detection of the Fe^{3+} was successfully in PMMA/CA polymer films. The sensitivity of the Fe^{3+} detection in PMMA/CA film was tested as well. In addition, the sensing abilities of the sensors in PMMA/CA film toward S^{2-} was also tested.

2.1.1 Phenanthroline Sensor in PMMA film for detecting Fe^{3+} (Task 2.1)

2.1.1.1 Preparation of the phenanthroline sensor and the Fe^{3+} solution

The Phenanthroline sensor (as shown in Fig. 2(a)) solution was prepared by dissolving Phenanthroline (0.1 g) in EtOH (19.9 mL). The solution concentration prepared is 0.5%. To prepare the Fe^{3+} solution, $FeCl_3$ was dissolved into distilled water. The concentration of Fe^{3+} solution is 5%. Fig. 2 shows that when the Fe^{3+} solution was slowly added into the phenanthroline sensor solution, the colorless phenanthroline sensor solution immediately changed to brown, indicating that the phenanthroline sensor is effective to detect Fe^{3+} in a solution environment.

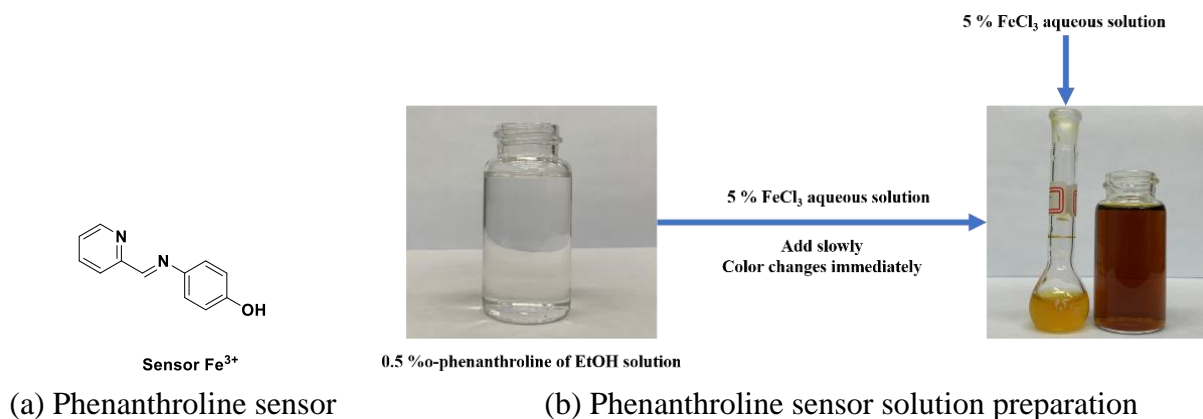


Fig. 2. Fe^{3+} added into phenanthroline sensor solution

2.1.1.2 Detecting Fe^{3+} in PMMA film on glass substrate

To prepare the phenanthroline sensor into the PMMA film, 1.8g of Poly(Methyl Methacrylate) Isotactic (PMMA) was added into 4.5 mL of the Tetrahydrofuran (THF), followed by stirring at room temperature until they completely dissolved in the THF for a colorless liquid. The dichloromethane (DCM) solution of phenanthroline (0.2 g) was added into the PMMA solution and stirred overnight as shown in Fig. 3. The mixture was then evenly spread on a clean glass surface and let dry in a ventilated place for two days. When the solvent evaporated, a transparent and colorless film was obtained.

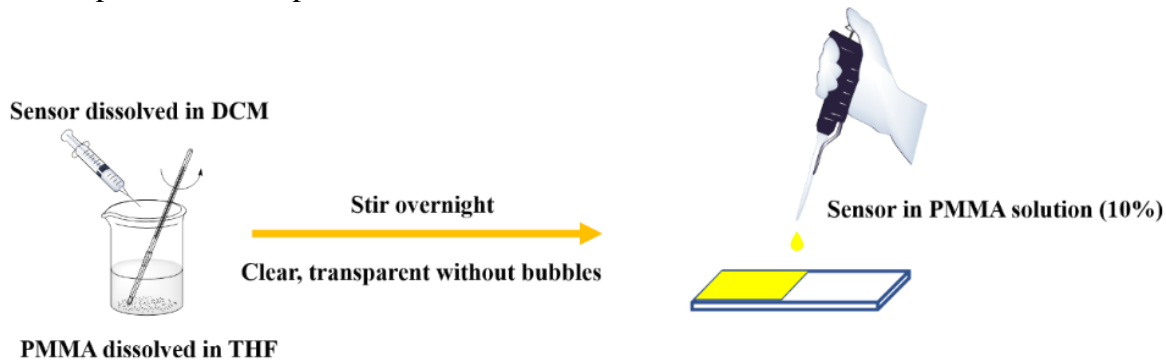


Fig. 3. Preparation of Phenanthroline sensor in PMMA film

The PMMA film with embedded phenanthroline sensor was then divided into four segments. Fe^{3+} solutions with different concentrations were dropped onto the different segments as shown in Fig. 4. The PMMA film with embedded phenanthroline sensor only showed significant color changes when the concentration of the Fe^{3+} solution reached 5%. A slight color change when the Fe^{3+} solution concentration reached 1%.

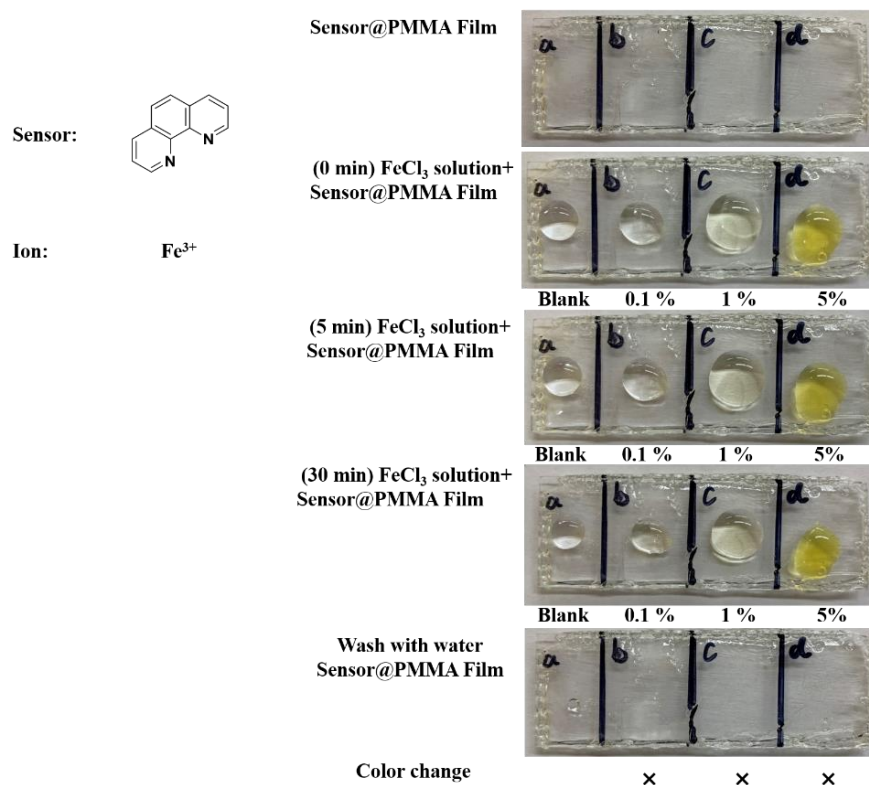


Fig. 4. Phenanthroline Sensor in PMMA film on glass substrate for detecting Fe^{3+}

To approve that the phenanthroline sensor into the PMMA film can sense Fe^{3+} with 5% of concentration in

a long term, the PMMA film with embedded phenanthroline sensor was immersed in 5% Fe^{3+} solution for one week and obvious color change was observed as shown in Fig. 5.

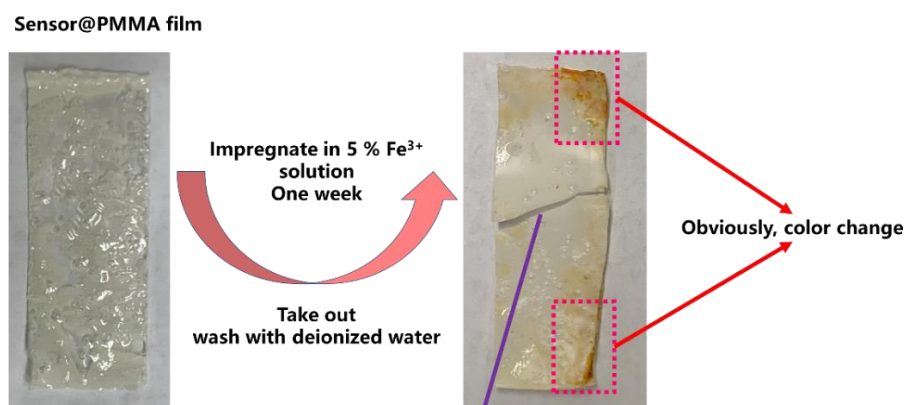


Fig. 5. Sensing test of a PMMA film with embedded sensor immersed in 5% FeCl_3 aqueous solution for one week

2.1.1.3 Detecting Fe^{3+} in PMMA film on steel substrate

To test the effectiveness of the phenanthroline sensor into the PMMA film (dopant content: 10%) on steel substrate, the PMMA film with sensor was coated on the steel surface and was dried in air for two days. The Fe^{3+} solutions with different concentrations were dropped onto the different regions of the PMMA film with embedded sensor on the steel surface. The color of film only showed with Fe^{3+} concentration larger than 5%, however, the color change was not obviously with the dark background of the steel substrate as shown in Fig. 6.

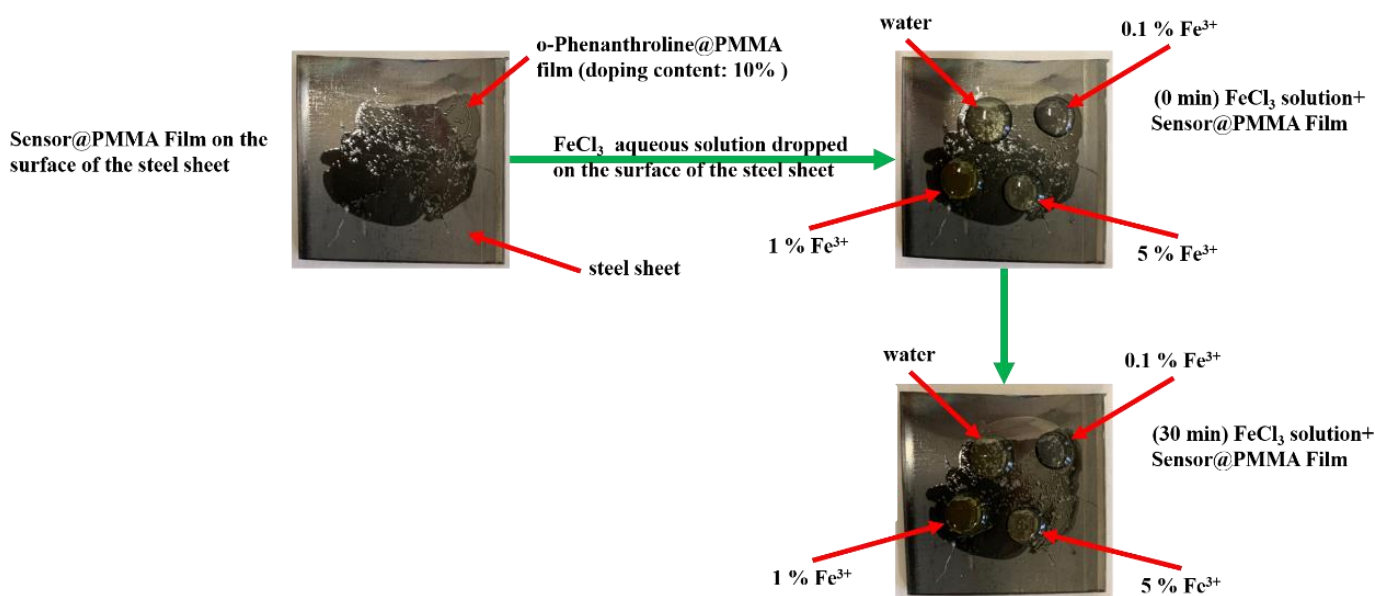


Fig. 6. Sensing test of phenanthroline@PMMA films coated on a steel sheet surface for Fe^{3+} sensing.

Thus, improvements are needed to make the coating working well. In this case, white paint is proposed to be added into the PMMA to improve the capability of the sensor color changes shown on steel substrate and also more porous material is needed for a better sensitivity below 1% of Fe^{3+} concentration. To improve the porosity, cellulose acetate (CA) is proposed to be added into the PMMA material to improve the porosity.

2.1.2. Phenanthroline Sensor in CA film and PMMA/CA film for detecting Fe³⁺ (Task 2.1 and Task 2.2)

2.1.2.1 Preparation of Phenanthroline sensor in CA and PMMA/CA film

The CA film was prepared by mixing 15 wt% CA (2 g) in 55 wt% DMF (7.33 g) and 30 wt% hexane (4 g) at 85 °C to form a homogeneous casting solution. To embed the sensor in the CA film, 500 mg phenanthroline was added. The solution was stirred for 20 min at 85 °C. A thin CA film with embedded sensor was then casted on a glass surface inside a hot chamber at 85 °C. The CA film with embedded sensor was covered by a glass container and left at room temperature for cooling. The glass substrate with the CA film was then immersed in a room-temperature deionized (DI) water bath until the film was detached. The detached film was then taken out and kept in another fresh DI water bath for 24 h to remove any trace amount of solvent. The wet film was used directly for the sensing test.

The PMMA/CA film was prepared in a similar way as used for the CA film preparation, except for that the mixed solution contained 7.4 wt% PMMA (1 g), 7.4 wt% CA (1 g), 59.3 wt% DMF (8 g), and 25.9 wt% hexane (2.5 g). To embed the sensor in the PMMA/CA film, 500 mg phenanthroline was also added. The rest of the sensor preparation is similar as the CA film with embedded sensor. To improve the sensitivity of the PMMA/CA film for color changes, white paint was added into the film for a better sensing indication.

2.1.2.2 Detecting Fe³⁺ in CA and PMMA/CA films and calibration of detection

The detached wet CA and PMMA/CA films with embedded phenanthroline sensor were divided into four segments and immersed into Fe³⁺ aqueous solutions with different concentrations for one week. As shown in Fig. 7, the CA films with embedded sensor showed a slight color change after one week with different concentrations of the Fe³⁺ ion ranging from 0%, 0.1%, 1%, and 5% as shown on the left group in Fig. 7.

On the other hand, the PMMA/CA films with embedded phenanthroline sensor showed significant color changes Fe³⁺ ion ranging from 0%, 0.1%, 1%, and 5% as shown on the right group in Fig. 7. The color change is significant to be detected easily even with a Fe³⁺ concentration of 0.1%, indicating a very effective sensor film for Fe³⁺ sensing. The resolution of the sensor can be as low as 0.1% of concentration and the sensitivity of the sensor is very promising.

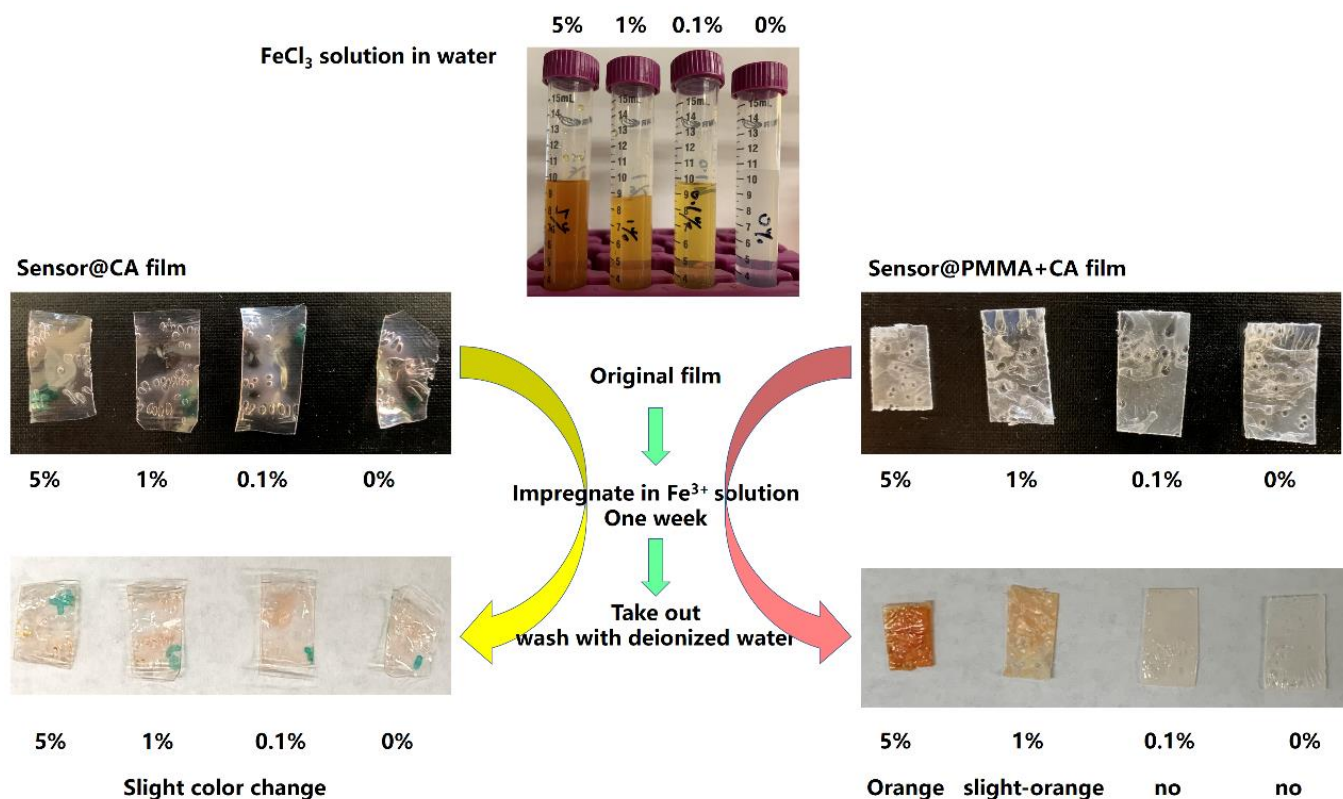


Fig. 7. Detecting Fe³⁺ in CA and PMMA/CA films with embedded sensors.

2.1.3 PMMA/CA films with embedded sensor for detecting S²⁻ (Task 2.1)

The PMMA/CA solution was prepared by mixing 7.5 wt% PMMA (1 g) and 7.5 wt% CA (1 g) in 55 wt% DMF (7.33 g) and 30 wt% hexane (4 g) at 85 °C to form a homogeneous casting solution. The solution was stirred for 20 min at 85 °C. Each sensor (100 mg) as shown on the left in Fig. 8. was dissolved in DMF (0.5 mL), and the solution (0.5 mL) was added into PMMA/CA solution (2 mL). The resulting mixture was stirred for 10 min to obtain a homogenous solution. The procedure followed the same as CA film made in previous section. The wet films with embedded sensor obtained are shown on the right in Fig. 8.

The PMMA/CA film with embedded sensor was divided into four segments and were immersed in different ion solutions with varied concentrations for one week. As shown in Fig. 9, the colors of PMMA/CA films with embedded sensor immersed in S²⁻ ionic solution didn't changed obviously after one week. Thus, improvements or new film materials are needed to be searched for detecting S²⁻ ion.

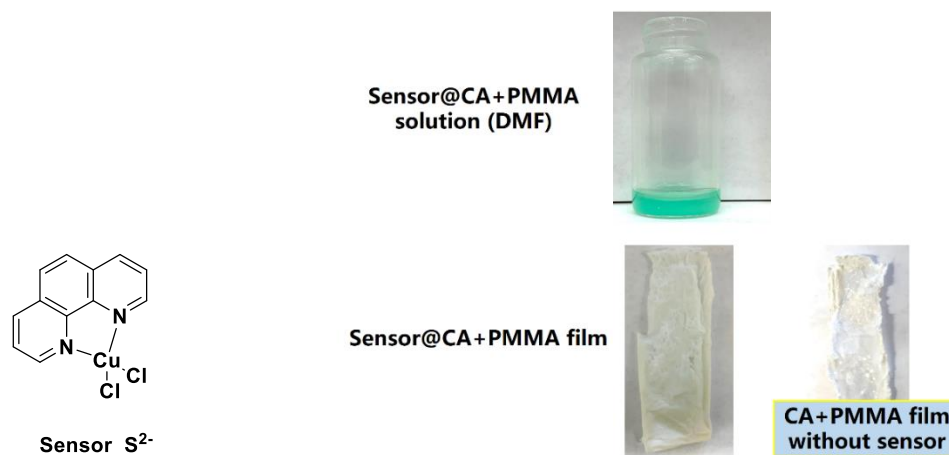


Fig. 8. PMMA/CA thin films loaded with sensor for detecting S²⁻ ion.

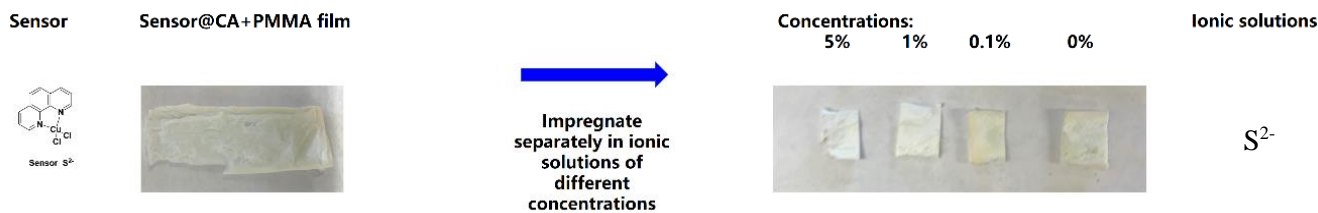


Fig. 9. Sensor response of PMMA/CA films immersed in solutions with different concentrations of S^{2-} for one week.

To sum up, based on the test results from last quarter and this quarter, films with embedded sensors to detect $CO_3^{2-}/Fe^{2+}/HCO_3^-$ and Fe^{3+} were successfully developed. In next quarter, focuses on Task 2.1 will be to develop films for detecting S^{2-} and H^+/pH .

2.2 Calibration of the Fluorescent/colorimetric Chemical Sensor Array (Task 2.2)

2.2.1 Sensor Array Survivability in Oil/Water Environment

2.2.1.1 CFD Model Analysis in Oil/Water Environment

In this quarter, we calculated the force applied on the sensor by oil-water two phase flow in a horizontal straight pipeline, which can be used to help optimize the geometry design of sensor for different purposes. The 2D and 3D model results were first compared and then 2D model was used for preliminary analysis to save computation time. Currently, it was assumed that full bonding exists between sensor and pipe wall and fluid-structure interaction can be neglected. Future work will be conducted to consider the bonding condition between sensor and pipe wall.

Comparison between 3D and 2D models: Although 3D model can generate accurate results, it requires significant amount of computation time. Therefore, 2D and 3D model results were compared for their differences. Fig. 10 shows the maximum wall shear stresses at different flow velocities obtained from 2D and 3D models. The results show that 2D models may cause slightly greater stress than 3D models, but their trends are similar. Therefore, 2D models was used in the preliminary analysis. After that, 3D models will be built for calculating accurate stresses.

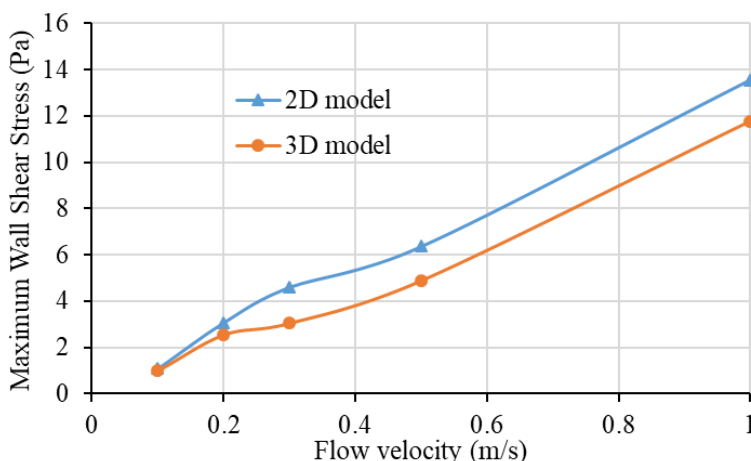


Fig. 10. Comparison of 2D and 3D model results

Pipe model with sensor attached: The pipeline analyzed in this study was assumed to be horizontal with a diameter of 0.1m and a length of 1m. The sensor was assumed to be located at the center bottom of the

pipeline with a dimension of 20mm by 10mm. In the current simulation, the sensor was modelled as the shape changes in the pipe wall. In this case, fluid-structure interaction was not needed. Fig. 11 shows the mesh details of model. The two-dimension model contains 26,562 elements.

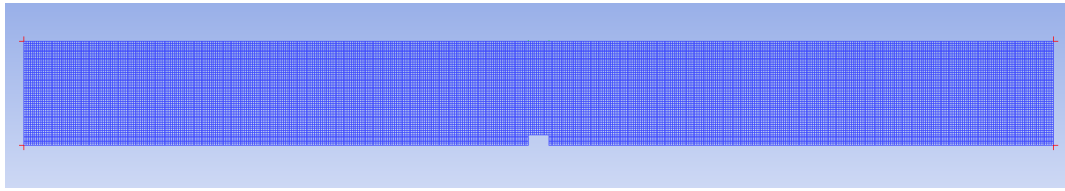


Fig. 11. Mesh of 2D model

The fluid flow was considered as transient and the effect of temperature fluctuations on the fluid flow was negligible. The Canadian crude oil with density of 914 kg and viscosity 37.2 cSt at 40°C was used for simulation. The water/oil weight percentage was 40% for water and 60% for oil. The operating pressure was set as atmospheric pressure. The fluid flow velocities of 0.2 and 0.5 m/s were considered. The CFD simulation used VOF model for two-phase flow. The velocity is below 0.5 m/s and the fluid could be treated as laminar fluid.

For the inlet of the pipeline, the velocity inlet was applied, the velocity of mixture was 0.5 m/s and the volume fraction of oil was 60%. For the outlet of the pipeline, the pressure outlet was used. The wall boundary condition was used to restrain the liquid. The simulation was time-dependent (transient) with 500 time steps, a time step was 0.01s and 40 iterations at each time step size.

Preliminary results and analysis: Figs. 12 and 13 show the velocity vector around the sensor and in pipe, respectively. The direction of the line shows the direction of flow and the color indicates the velocity value. It was found that water flew diagonally upward at the sensor and caused vortex behind the sensor.

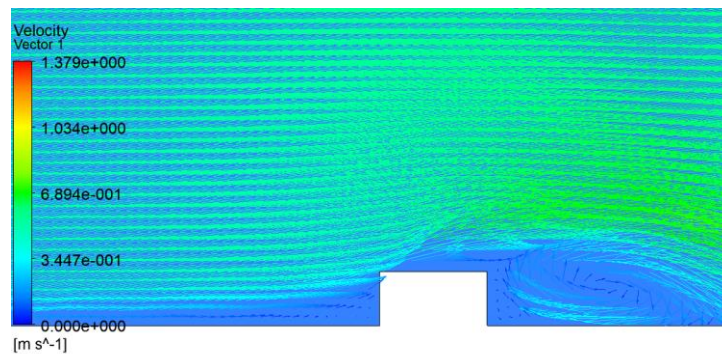


Fig. 12. Velocity vector around the sensor

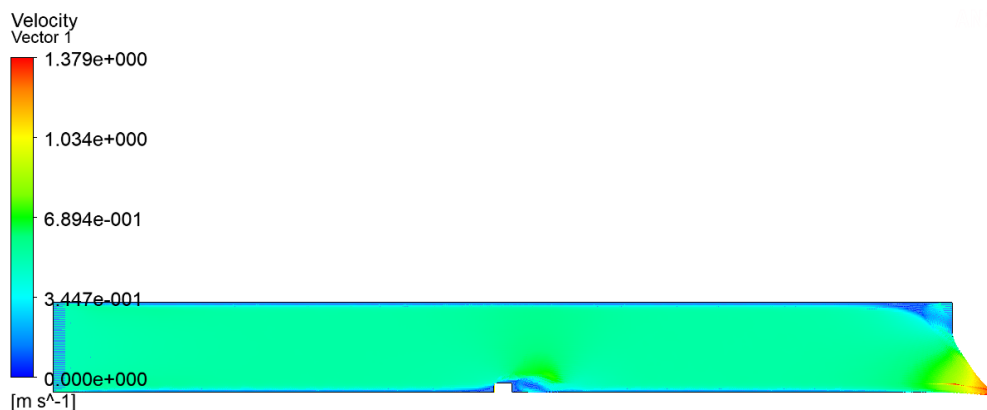


Fig. 13. Velocity vector in the pipeline

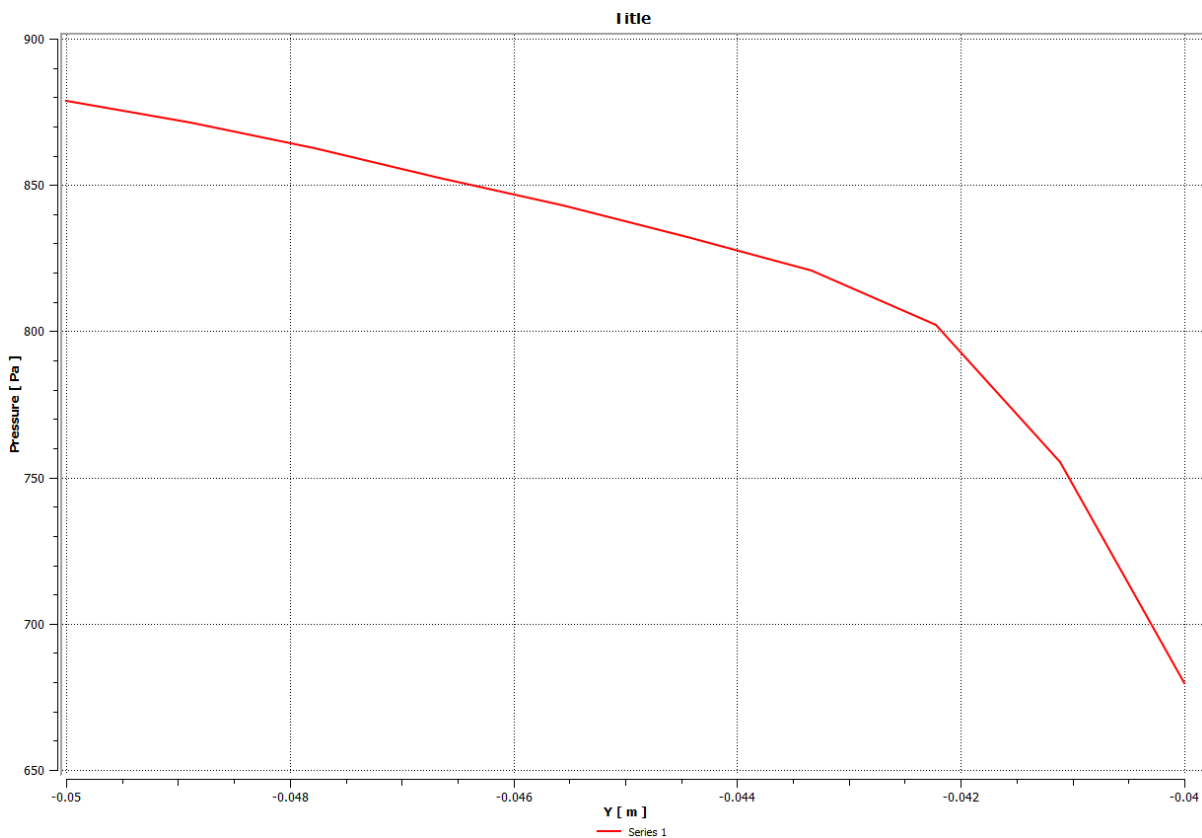


Fig. 14 Pressure on the vertical wall of sensor

Fig. 14 shows the induced pressure by the flow at different depths on the left vertical wall of the sensor. The force can be calculated as the area formed by the curve. The total force on the sensor was about 8.23N. In Section 2.2.2.3, the simulation results for a sensor attached on the pipe internal surface with the passing of a cleaning pig show that the force induced by the pass of a cleaning pig is 100N. Compared with the simulated results from the flow with 8.23N, the force from the pass of a cleaning pig is significantly larger, which is 10 times larger. Thus, in the survivability test, the assumption that the sensor survivability was controlled by the passing of a cleaning pig is a valid assumption for the sensor design and optimization.

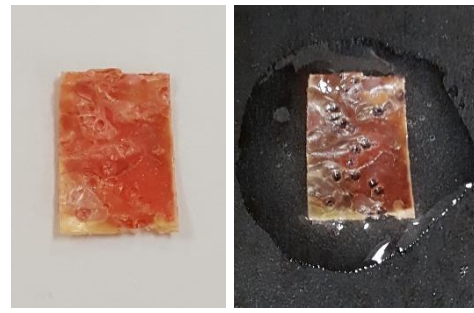
2.2.1.2 Experimental Testing of Sensor Survivability under Atmospheric/Oil Condition

To test whether the sensor can survive or need a cleaning service, the first series of the tests was conducted under atmospheric/oil condition. Due to the fact that the sensor film was pre-fabricated, the sensor film was attached on the n the internal surface of steel pipes using epoxy. No surface treatment was performed on the steel pipe surface before the attachment of the sensor film. Fig. 15 (a) shows an original sensor film and the attached sensor film on the steel pipe inner surface using epoxy without reacting with 5% of Fe^{3+} in the air without placing it in the gasoline. Fig. 15 (b) illustrates an sensor film reacted with 5% of Fe^{3+} in the air and an attached sensor film on the steel pipe inner surface using epoxy reacted with 5% of Fe^{3+} in the air without placing it in the gasoline.

To test whether cleaning service is needed for sensor film in oil/gas environments, one sets of pipes with attached sensor film samples as in Figs. 15 (a, b) were placed into gasoline and another sets of the pipes with attached sensor film samples were not placed into gasoline. Figs. 15 (c) and (d) illustrate the corresponding sensor films after placing in and taking out from gasoline. Comparing Fig. 15 (a) and (c), it can be seen that the sensor film appearance did not change with immersing or not into gasoline. The comparison between Fig. 15 (b) and (d) shows that the gasoline would not impact the sensor film's performance when Fe^{3+} ion presented. Thus, cleaning service is not needed for the sensor to work in practice.



(a) PMMA/CA film with embedded sensor



(b) PMMA/CA film with embedded sensor immersed into 5% Fe^{3+} solution



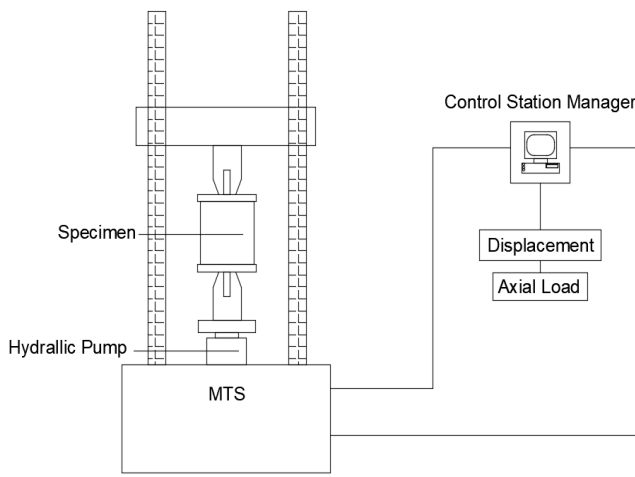
(c) PMMA/CA film with embedded sensor after taken out from gasoline



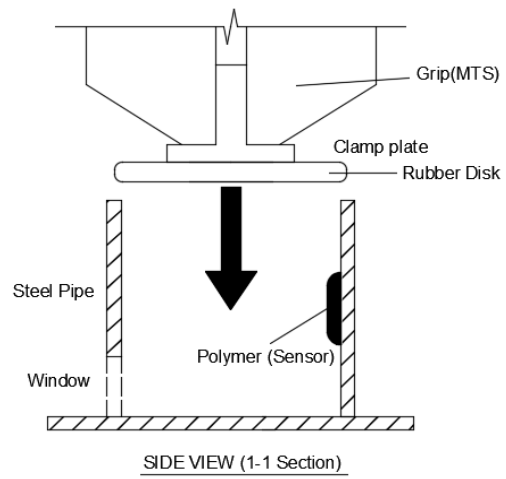
(d) PMMA/CA film with embedded sensor immersed into 5% Fe^{3+} solution after taken out from gasoline

Fig. 15. Test sensor film samples

To test the survivability of the sensor film and the impact of cleaning service on the color changes of the sensor film, a laboratory test of a simulated passage of a cleaning pig was performed on all those four samples as shown in Fig. 15. Fig. 16 shows the test design of passing of a cleaning pig. Specifically, the traveling portion of a typical PIG is made up of a rigid and hollow center body and two sets of sealing disks. Clamp plates are used to hold each sealing disk in place on either side of the main rigid body. The PIG with sealing disks made of polyurethane rubber is usually propelled down the line due to the flow in the pipeline. In this research, according to the actual procedure of pigging service, a rubber disk made of polyurethane and steel pipes with 6'' was selected as test specimens to simulate the pigging process. MTS hydraulic loading machine was used to drive the rubber disk through the pipeline, and the equipped data collection system could record the axial load and displacement of the lower loading Grip. So that the friction on the inner pipe walls, the sensor and whatever the force preventing the pigging motion would be recorded for further analysis.



(a) The Experimental arrangement



(b) Test part sketch

Fig. 16. Experimental design of simulated passage of a cleaning pig

Fig. 17 show the appearances of sensor film samples after the tests. Figs. 17 (a) and (b) illustrate that the cleaning procedure doesn't change the appearance of the colored sensors. When comparing Fig. 15 (c) with Fig. 17 (c), it can be seen that the immersing of the sensor film (without reaction with Fe^{3+} ion) in gasoline did not change the appearance of the sensor film. The comparison between Fig. 15 (d) and Fig. 17 (d) indicates that in the condition after the sensor film detected Fe^{3+} with color changes, the gasoline did not change the appearance of the sensor film.



(a) Attached sensor film after test without gasoline



(b) Attached sensor film after test without gasoline



(c) Attached sensor film after test with gasoline



(d) Attached sensor film after test with gasoline

Fig. 17. Sensor's performance in service conditions

Based on the test results, the following findings can be summarized:

- 1) The developed PMMA/CA sensor film can survive gas/oil in atmospheric condition;
- 2) The color change stayed unchanged after immersing the sensor film in gas/oil in atmospheric condition, indicating that no cleaning service is needed for the application of the detection of color

changes of the sensor film;

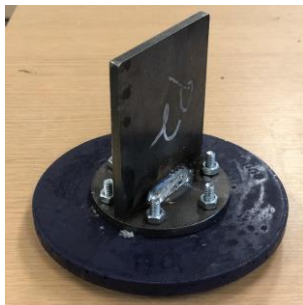
- 3) The attached sensor film maintained their physical body intact under mechanical scratching from the rubber disk, indicating good physical stability to survive cleaning activities;
- 4) The cleaning process did not disturb the color change of the sensor film, showing the sensor film could survive and maintain functional when a cleaning/inspection pig passing.

2.2.2 Sensor Film Survivability with Passing a Cleaning Pig (Task 2.2 and Task 2.3)

Based on the designed tests from last quarter which also shown in Fig. 16 in last section, experiments were performed on PMMA/CA sensor film under PIG activities. The PMMA/CA sensor film was approved to be effective detecting Fe^{3+} ion in this quarter based on Section 2.1. In addition, equivalent finite element model (FEM) simulation were updated based on the new manufacturing procedure of the sensors.

2.2.2.1 Laboratory Experiment on Sensor Film Survivability with Passing a Cleaning Pig (Task 2.2)

Sample Preparation and Test Setup: Pigging is now a standard procedure in petroleum and natural gas industry. Fluid or gas is pumped upstream to provide necessary force for cleaning the wax and sediments or dewatering. The test setup shares the same as in Section 2.2.1.2 and in Fig. 16. The fabrication of the samples with PMMA/CA sensor films attached is shown in Fig. 18. As the same with devices used in the last quarter, 6' in. pipeline and corresponding rubber disk were adopted in the test as shown in Fig. 18. The test parts were arranged as experimental design in Fig. 16. In an MTS movement procedure, the upper grip was fixed with vertical movement, tightly grasping the T-shape PIG disk with a 25'' occlusion length. In the meanwhile, the lower grip was moving upwards so that the rubber disk could go inside the pipe to restore the actual cleaning progress. The clean space for the pipe to move upwards was 75mm. A 2-way movement was applied in the test to let the disk move bidirectionally in the pipe, to make sure the sensors attached on the inner wall could survive the cleaning process from two directions.



(a) 6" rubber disk



(b) 6" steel pipe



(c) Test setup

Fig. 18. Devices in laboratory tests

To drive the disk smoothly, protect the rubber, and get stable experimental data, a displacement-control program was set to the hydraulic loading machine. The test parameters were shown in Table 1, in which Initial Displacement means the gap between the starting point and the contact point at the pipe was 5mm. The two-way tests were divided into two independent parts for data collection (Displacement and Axial load), and in each test, a 50Hz sampling rate was adopted to have dynamic record of axial displacement and axial load.

Table 1. Test Setup Parameters

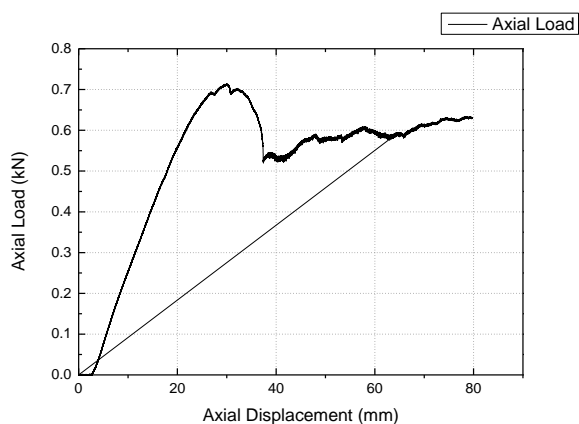
Parameter	Value
Control mode	Displacement

Displacement mode	Monotonic
Initial displacement	-50mm
Displacement rate	0.2mm/s
Absolute displacement	± 75 mm (two-way)
Sample rate	50Hz

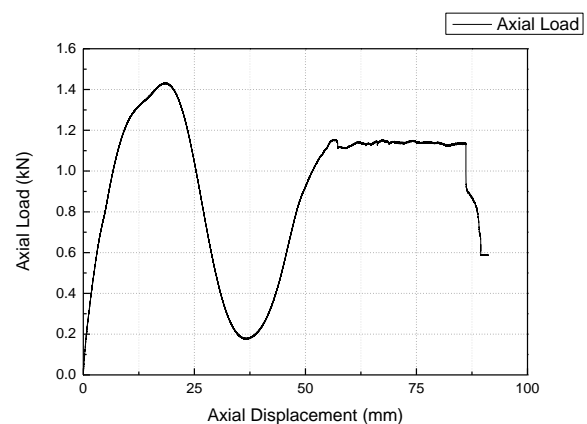
Test Results and Discussions: During the test process, axial displacement and load were recorded through program for the calculation of the friction on sensors. The curves were categorized into two parts, correlated with two moving directions of the rubber disk. As known from the previous outcome, the friction applied on the sensors were controlled by sensor thickness. So, sensors with the same thickness but different chemical treatment have the same mechanical responses under rubber movements. In this study, curves in atmospheric and gasoline condition are shown in Fig. 19. Each of them was divided into disk moving-in and moving-out process.

The same trend was found in Fig. 19 compared to the test for plain pipe surface in last quarter. The curve can be categorized into two stages for the two-stage rubber disk deformation. Stage 1 is the deformation outside the steel pipe, in which the rubber disk deforms because of its oversized outer edge. After the certain point of the axial displacement that is the start point of Stage 2, the oversized disk is completely squeezed into the pipe, from where the stable slip motion would happen, and the axial load is to overcome the friction between the disk and the pipe. It is shown from the curve that in the deformation Stage 1, the axial load showed a fluctuation characteristic which reached a high value and then re-raise to a specific value and then entered the deformation Stage 2. In the Stage 2, which axial load remained stable, axial load was considered as friction only. The axial load increased when the disk passes through the sensor's surface, so that the increasement of axial load can be seen as taken by the sensor film. Thus, from the recorded axial load, different friction on sensor films in different thickness could be calculated for the shear force for a sensor to survive.

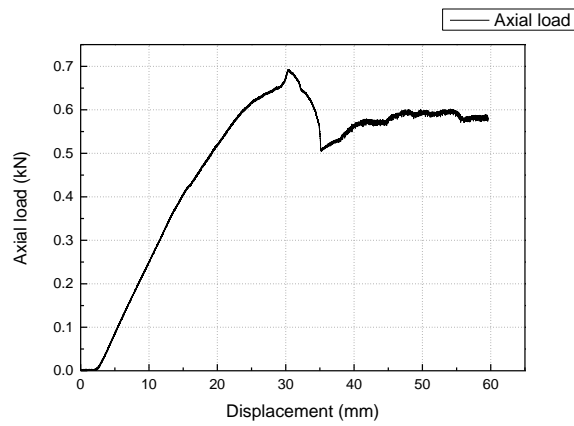
Based on Figs. 19 (a, b), for sensor film without immersing in gasoline, the axial load reached 630 N as the maximum load when the disk was moving inside the pipe. In the moving out process, the maximum axial load is 600 N calculated from Fig. 19 (b). For sensor film immersed in gasoline, the two maximum axial load values are 600 N and 550 N based on the same calculation method. From a rough sketch of the curve, it can be concluded that the presence of gasoline act as lubrication because of the decrease of the overall axial load.



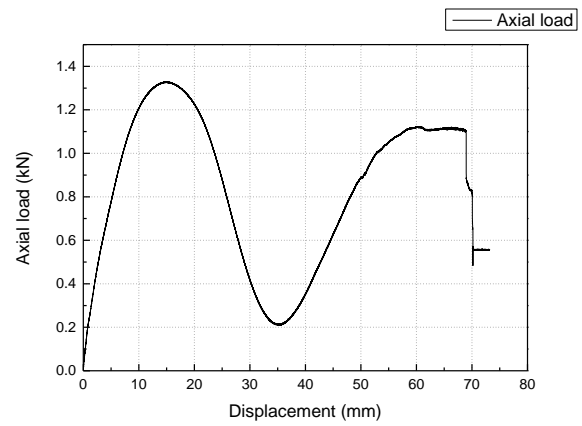
(a) Load-displacement curve of sensor film without immersed gasoline (disk moving in)



(a) Load-displacement curve of sensor film without immersed in gasoline (disk moving out)



(c) Load-displacement curve of sensor film immersed in gasoline (disk moving in)



(d) Load-displacement curve of sensor film immersed in gasoline (disk moving out)

Fig. 19. Load-displacement curve

2.2.2.3 FEM Simulation Analysis for Sensor Survivability and Size Optimization (Task 2.2 and Task 2.3)

FEM Model Setup: Based on the experimental parameters in last section, the existing Finite Element Model (FEM) was updated with the PMMA/CA sensor film parameters. The sensor film was modeled as a polymer base, adding a thin layer of epoxy to attach sensor to steel substrate. The profile of the model is shown in Fig. 20. The outer diameter of the steel pipe was assumed to be 154mm (6 inches) with a thickness of 7mm. Regular A36 steel was used as steel pipe material in the analysis. The disk on the cleaning pigs, was built to have a thickness of 13mm and a diameter of 147 mm, which is 5% oversized when compared with the inner diameter of the pipe. The material of the sealing disk was assumed to be polyurethane rubber. The thickness of the clamp plates was 6.4mm with an outer diameter of 76.2mm, which correspond with experimental arrangement (Fig. 16). The displacement setting remained the same as the previous simulation setup.

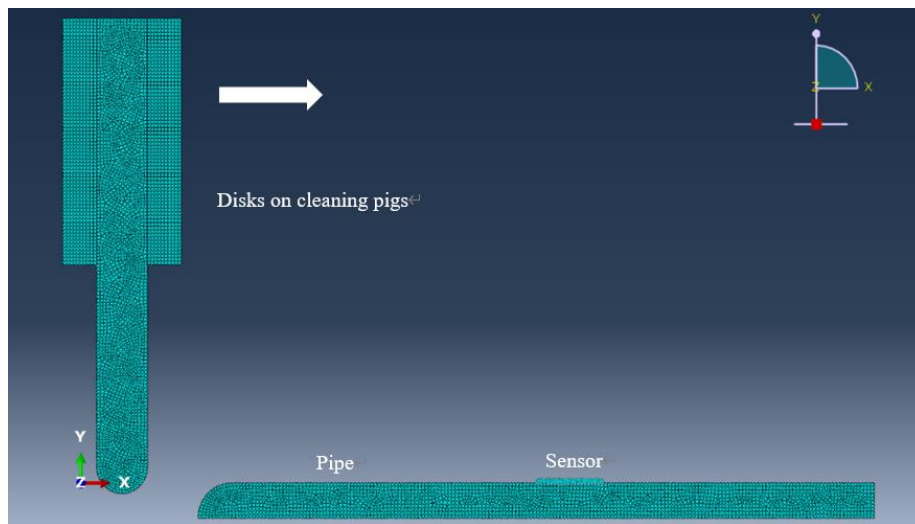


Fig. 20. FEM model

Simulation Results: As the simulation results from the previous reports, the disk deformed when it was going through the pipe. The presence of the sensor film on the inner surface of the pipe restricted the disk's deformation leading to a greater bending and higher stress in the rubber disk. It also resulted in a higher friction stress in the sensor base and steel substrate as seen in Fig. 21.

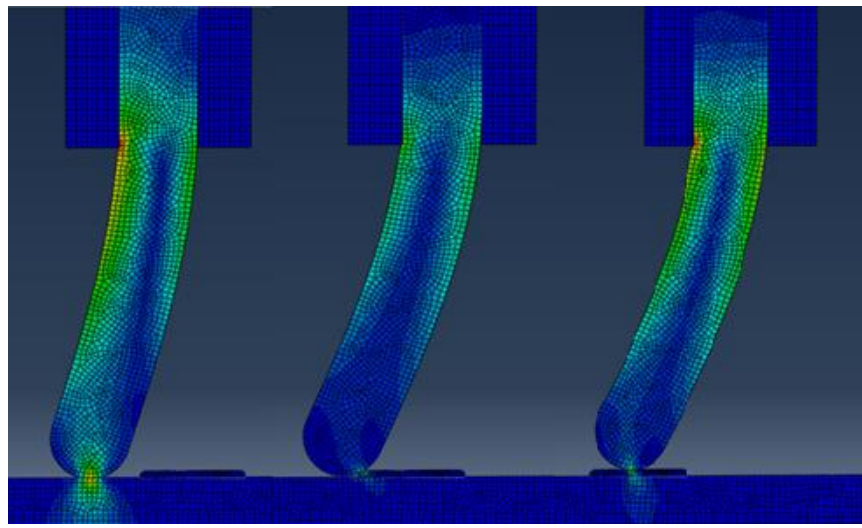
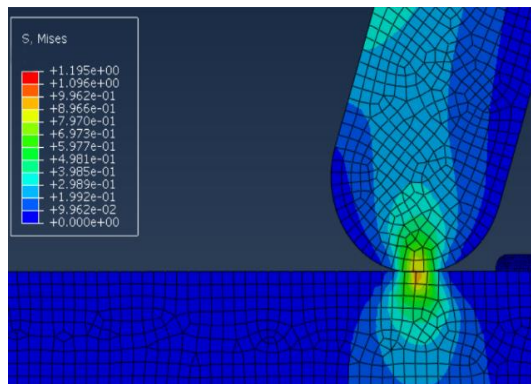
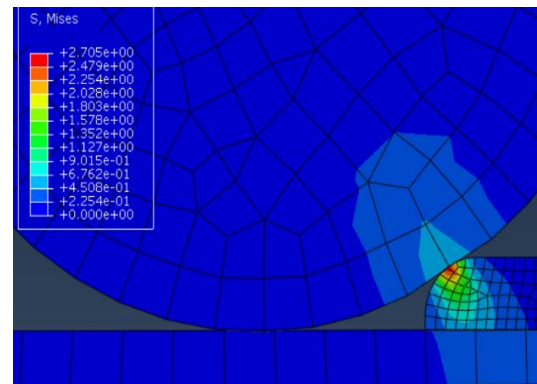


Fig. 21. FEM deformation results.

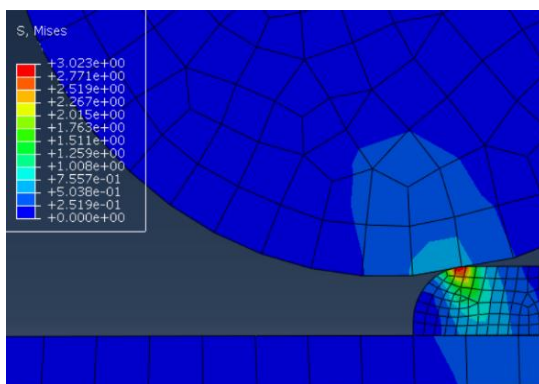
To calibrate the simulated result with experimental result, a stress field correlated with the axial load was exported as shown in Fig. 22. The maximum stress presented on both the sensor and the rubber disk was 3.023 MPa, which was exactly the same with the 1mm thickness sensor from the previous report. In addition, the stress between rubber disk and steel pipe, stress during climbing also remained the same. This indicated that the interaction between sensor film and rubber disk was determined by the size of the disk and thickness of the sensor, which were all dimensional parameters. The maximum stress remained the same when the component of the sensor changed as long as the thickness kept unchanged. So, the primary consideration of the stress field inside the sensor was thickness but not the sensor materials. However, a reliable bond between the sensor and pipes is needed to make this assumption sustain.



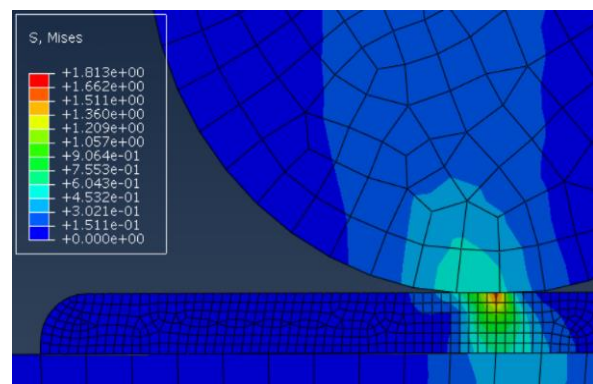
(a) Before contact



(b) In contact



(c) Climbing



(d) Scratching

Fig. 22. Mises stress in the sensor from FEM analysis

Discussions: The experimental results in Section 2.2.1.2 from the PMMA/CA sensor film showed that the sensor film can survive the passing of the rubber disk with sensor film either in atmospheric or immersed into gasoline before tests. However, a unified metrics is still needed for calibration the test and simulated results. To convert the axial load into stress in sensors, a conversion relationship should be established for verification purpose of the two approaches. Under the circumstance of the in-progress experiments and simulation, a conversion relationship was chosen for the first-step validation. With the assumption that the contacting area of the disk and the pipe was a circular ring, the shear stress could be calculated by Equation (7) in which F is Axial load given by the experimental tests:

$$\tau_{sensor} = \frac{F}{A_r} \quad (7).$$

where, F is the axial load of experimental results, and A_r is the area of the contacting area which can be calculated as below:

$$A_r = l \times d \quad (8)$$

where, l is the contacting length between the disk and the sensor, and d is its width.

In the laboratory experiments, the rubber disk had a chamfered edge when contacting with the steel pipe. So, a 2 mm contacting area width as assumed from the simulation result (mesh dimension of the rubber disk was 1 mm/cube) and a 15mm length as measured in experimental tests were adopted to calculate the corresponding stress. The experimental tests in the previous report indicated that 540 N load was detected when disk went through the pipe without sensors. Combining with the maximum load in this report, which is 630 N, 90 N of the axial load was induced by the presence of sensor. This means the sensor carried a force of 100 N when the disk passed through the sensor. After acquiring all the parameters needed, the stress in the sensor under experimental condition (without gasoline) is 3.00 Mpa as calculated, which shows well correspondence with the simulated stress result (3.023 MPa). The Finite Element Model can be used for reliable sensor optimization in future.

2.2.3 Integration of Corrosive Water into Internal Corrosion Prediction Models (Task 3)

2.2.3.1 Prediction Model of Sweet Corrosion

To establish the relationship between corrosion environments and the prediction models, numerical and mechanistic models will be introduced in this project. Based on the literature, numerous corrosion prediction models for steel with presence of carbon dioxide exists, including mostly empirical or semi-empirical models. While, some of the recent models are based on mechanistic description of the process underlying CO₂ corrosion. Very different results can be obtained when the models run for the same cases due to the different philosophies used in the development of the models. Some of the models predict corrosion rates based on full water wetting and little protection from corrosion product films. These models have a built-in conservatism and can over-predict the corrosion attack significantly for many cases. The most popular used corrosion models for sweet corrosion, which is also known as basic models, include the electrochemical model [4] and GDN (George, de Waard, Netic) model [5].

Electrochemical Model: The electrochemical model assumed that the main cathodic reaction is introduced by the H⁺ reduction and the H₂CO₃ acts primarily as additional sources of H⁺ ions (through dissociation). The only anodic reaction considered below is the iron dissolution. Hence, the current density vs. voltage equation for H⁺ reduction can be presented as:

$$\frac{1}{i_{(H^+)}} = \frac{1}{i_{a(H^+)}} + \frac{1}{i_{\text{lim}(H^+)}^d + i_{\text{lim}(H_2CO_3)}^r} \quad (9)$$

where $i_{(H^+)}$ is the charge transfer current density in A/m^2 , $i_{\text{lim}(H^+)}^d$ is the mass transfer limiting current density for H^+ ions in A/m^2 , and $i_{\text{lim}(H_2CO_3)}^r$ is the chemical reaction limiting current density arising from the presence of H_2CO_3 in A/m^2 . The charge transfers current density in Equation (9) is given by the Tafel relationship:

$$i_{a(H^+)} = i_{0(H^+)} \times 10^{-\frac{\eta}{b_c}} \quad (10)$$

in which $i_{0(H^+)}$ is the exchange current density in A/m^2 , η is the overvoltage in V, and b_c is the cathodic Tafel slope in V/dec. The H^+ mass transfer limiting current density in Equation (9) can be calculated by:

$$i_{\text{lim}(H^+)}^d = k_m F \{H^+\}_b \quad (11).$$

The H_2CO_3 chemical reaction current density in Equation (9) can be calculated as:

$$i_{\text{lim}(H_2CO_3)}^r = F [CO_2]_b \sqrt{D_{H_2CO_3} K_{hyd} k_{hyd}^f f} \quad (12)$$

where $F[CO_2]_b$ is the bulk concentration of carbon dioxide in $kmol/m^3$, $D_{H_2CO_3}$ is the diffusion coefficient of H_2CO_3 in m^2/s , K_{hyd} is the equilibrium constant for carbon dioxide hydration s^{-1} , k_{hyd}^f is the rate of hydration of carbon dioxide in s^{-1} and f is the flow multiplier. The only anodic reaction considered, iron dissolution, was assumed to be under activation control and hence pure Tafel behavior was modeled. The current density vs. voltage equation can be given as:

$$i_{(Fe)} = i_{0(Fe)} \times 10^{\frac{\eta}{b_a}} \quad (13)$$

where $i_{0(Fe)}$ is the exchange current density in A/m^2 , η is the overvoltage in V, and b_a is the anodic Tafel slope in V/dec. The corrosion potential then is found by solving the charge balance equation at the metal surface:

$$i_{(Fe)} = i_{(H^+)} \quad (14)$$

Direct reduction of water was neglected in the electrochemical model. Once the corrosion potential is obtained from Equation (13), the corrosion current can be found from the anodic current density (Equation 14) at the corrosion potential. For our application, since the output of the sensor film is color changes instead of current, this model is not applicable for our developed sensors.

GDN Model: The well-known GDN model was modified recently as shown below:

$$\frac{1}{V_{corr}} = \frac{1}{V_r} + \frac{1}{V_{m(H_2CO_3)}} \quad (15)$$

where V_{corr} is the corrosion rate in mm/yr, V_r is the reaction rate in mm/yr, and $V_{m(H_2CO_3)}$ is the mass transfer rate of H_2CO_3 in mm/y. The reaction rate in Equation (15) can be further written as:

$$\log(V_r) = c_1 + \frac{c_2}{T} + c_3 \log(pCO_3) + c_4(pH_{actual} - pH_{CO_2}) \quad (16)$$

in which, pCO_2 is the partial pressure of CO_2 in bar, pH_{actual} is the actual system pH in the presence of cations such as Ca^{2+} , Fe^{2+} , Mg^{2+} , etc., pH_{CO_2} is the pure pH of the system arising from CO_2 dissolution only and the c_1 to c_4 are constants. The H_2CO_3 mass transfer of the corrosion rate in Equation (16) can be found as:

$$V_{m_{H_2CO_3}} = c_5 \left(\frac{v^{0.8}}{d^{0.2}} \right) [pCO_2] \quad (17)$$

where v is kinematic viscosity in m^2/s , d is pipe diameter in m and c_5 is a constant.

Since our sensor film will not detect the CO_2 pressure in the oil/gas, the application of GDN model in our study is not applicable either.

Johnson and Tomson (JT) Model: There are also some other model expressions for the corrosion precipitation (crystal growth) rate. Some studies presented mathematical models which are the most of the important processes present in corrosion using fundamental physicochemical laws. The Johnson and Tomson (JT) model is one of them. Based on the JT model, the corrosion rate in the present of CO_3^{2-} and Fe^{2+} is shown in Equation 18:

$$R_{FeCO_3} = A \times e^{54.8 - \frac{123.0kJ/mol}{RT}} \times K_{sp} \times (S^{\frac{1}{2}} - 1)^2 \quad (18)$$

According to van Hunnik, et al., the expression of JT model can be modified as:

$$R_{FeCO_3} = A \times e^{52.4 - \frac{119.8kJ/mol}{RT}} \times K_{sp} \times (S - 1)(1 - S^{-1}) \quad (19)$$

In these two expressions (18, 19), A is the surface area available for precipitation per unit volume and K_{sp} is the precipitation rate constant, R is Boltzmann constant, and S represents the considerable supersaturation of Fe^{2+} or CO_3^{2-} ($S = c_{Fe^{2+}} \text{ or } c_{CO_3^{2-}} / K_{sp}$), where $c_{Fe^{2+}}$ and $c_{CO_3^{2-}}$ are the tested concentration of Fe^{2+} and CO_3^{2-} respectively. The solubility product (K_{sp}) for $FeCO_3$ is constant and modeled as a function of temperature ($^{\circ}C$). $FeCO_3$ precipitation has been implemented in the model as a chemical reaction taking place at the steel surface, in the porous corrosion film and on the film surface. The precipitation reaction acts as a sink for Fe^{2+} and CO_3^{2-} ions, influencing the fluxes and concentration gradients for both the ions and all other carbonic species. The model can predict the corrosion rate as well as the concentration and flux profiles for all species involved. In addition, it can be adjusted to the corrosion rate of other ions with little modification base on test results. Thus, in this project, we will develop a new-designed model Based on the JT model for the corrosion prediction purpose.

2.2.3.2 Test Plan of Selected Corrosion Prediction Model

By using the modified TJ model, a specific value of the corrosion rate under CO_3^{2-} condition can be calculated by measuring the concentration of Fe^{2+} and CO_3^{2-} ions inside the pipes. With the testing results from the developed sensors in this study, the sensitivity of the sensors can show the relationship between the indicating color and the concentration of the Fe^{2+} and CO_3^{2-} ions inside the pipes. The correlation between the ion concentrations to the corrosion rate can then be built, so that the definition of corrosion monitoring as well as protection can be established.

To correlate the concentration of ions (indicated by the color changes of the sensors) to the corrosion rate, experimental tests are needed. The test procedure is shown below (Fig.23). Firstly, solutions with different Fe^{2+}/CO_3^{2-} concentration are prepared for the color change test to determine the sensitivity of the sensor as in Task 2.2. Then, followed by a calibration of the corrosion rate and the ion concentration, a specific

correlation can be derived. Thus, the outcome of the developed sensors can quantify and predict corrosion rate, which is the basis of the further corrosion protection.

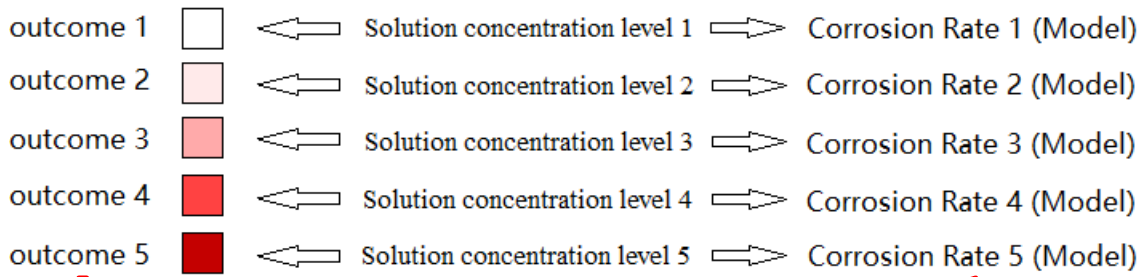


Fig. 23. Test plan of corrosion prediction models

2.3 Student Mentoring

During this quarter, four graduate students (Shuomang Shi, Ph. D. in Civil and Environmental Engineering at NDSU, Hafiz Usman Ahmed, Masters in Civil and Environmental Engineering at NDSU, and Jiapeng Lu, Ph.D. Student in chemistry at NDSU, Baiyu Jiang, Ph.D. in Civil Engineering at Rutgers University) and two undergraduate research assistants (Gina Blazanin and Alex Glowacki) were hired to work on this project. The four graduate students will work on this project from Quarter 5 to Quarter 6 of this project. The two undergraduate students were hired from October 2019 to December 2019. New undergraduate research assistants will be hired in January 2020 for the next quarter of this project.

2.4 Outreach Activities

On Oct. 25th, 2019 (8 am to 2 pm), an one-day outreach event named “Pipeline Challenge” workshop in BrainSTEM was conducted based on this project. This workshop intended to let the middle school students have hands-on experiences using easy tools to plan and build pipeline as shown in Fig. 24. A total of 45 middle school students attend this workshop. It is expected to encourage and generate interests for young kids to pursue pipeline engineering for future college education or careers. Table 2 is the schedule of the event.

Table 2 Outreach BrainSTEM Workshop Schedule

8:00	9:00	Presenter Arrival
9:00	9:25	Student Arrival
9:25	9:40	Welcome in Centrum
		<i>We would like you to join us for this if possible. We'll line up the presenters in the front and do quick introductions for the kids. I'd also like a group photo</i>
9:50	10:40	Session 1
10:50	11:40	Session 2
11:45	12:25	Lunch – Anderson Commons
12:30	1:20	Session 3



Fig. 24. Outreach photo

2.5 Future work

In the 6th quarter, there will be three objectives:

- 1) Task 2.1: Develop sensor film for the S^2 and H^+ /pH;
- 2) Task 2.2: Continue the simulation and experimental research on the survivability under oil/gas or water environment;
- 3) Task 2.2: Test the sensor film characteristics;
- 4) Task 2.3: Optimize sensor size based on sensor's survivability under PIG activities;
- 5) Task 3: Test parameters for corrosion model prediction.

References:

- [1] Nor Roslina Rosli, "The Effect of Oxygen in Sweet Corrosion of Carbon Steel for Enhanced Oil Recovery Applications", Ph.D. Dissertation, Ohio University, Dec 2015.
- [2] C. deWaard and D. E. Milliams, "Carbonic acid corrosion of steel," Corrosion, vol. 31, no. 5, pp. 177–181, 1975.
- [3] L. G. S. Gray, B. G. Anderson, M. J. Danysh, and P. R. Tremaine, "Mechanism of Carbon Steel Corrosion in Brines Containing Dissolved Carbon Dioxide at pH 4," in CORROSION/1989, New Orleans, LA, 1989.
- [4] S. Wang, K. George, S. Nestic, "High Pressure CO₂ Electrochemistry and the Effect of Acetic Acid", CORROSION/2004, Paper No. 04375, (Houston, TX: NACE International, 2004).
- [5] K. George, S. Nestic, K. de Waard, "Electrochemical Investigation of CO₂ Corrosion of Mild Steel in the Presence of Acetic Acid", CORROSION, Paper No. 04379, 2004.
- [6] Nordsveen, M., et al. "A mechanistic model for carbon dioxide corrosion of mild steel in the presence of protective iron carbonate films—part 1: theory and verification." Corrosion 59.5 (2003): 443-456.